Bio-Design and Manufacturing (2025) 8:410–422
https://doi.org/10.1631/bdm.2400424

RESEARCH ARTICLE

Vascularized organoid-on-a-chip for centimeter-scale organoid cultivation

Xiaofeng Gong[1,2] · Chen Yang[3] · Jianchen Peng[1,2] · Xiao Ding[3] · Hui Yang[4] · Aaron Gerald Wang[5] · Emmanuel Enoch Dzakah[6] · Bing Zhao[2,4,6]

Received: 20 October 2024 / Accepted: 2 December 2024

Abstract

An organoid is a three-dimensional (3D) cell culture model that can reproduce the distinct structure and inherent functionality of certain organs. Nevertheless, a major limitation of organoids is the absence of a complex vascular network, thus restricting the supply of oxygen and essential nutrients. Coupled with their inherent size constraints and metabolite accumulation, it is challenging for organoids to replicate the natural intricacies of organs, thereby limiting their applicability. To overcome the challenges associated with this technology, we developed a culture platform to cultivate tumors or organ-derived organoids up to the centimeter scale. Initially, a customized organoid-on-a-chip including a microvascular network at the micron scale was designed using 3D printing. Further, by integrating an infusion device, the chip ensures an adequate supply of nutrients and fluid immersion while mimicking blood flow dynamics. Our method overcomes the issue of the limited size of organoids due to insufficient nutrient access, making it possible to produce large-scale tumor and normal tissue models in vitro, while providing insights into drug efficacy and toxicology evaluation as well as standardized organoid production.

Graphical abstract

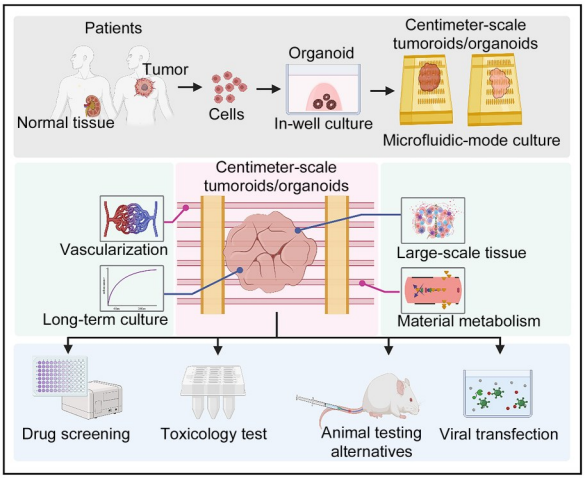

Keywords Organoid · Tumoroid · Biomaterials · Organoid-on-a-chip · Biomedical engineering

Xiaofeng Gong and Chen Yang have contributed equally to this work.

✉ Bing Zhao
bingzhao@ncu.edu.cn

1 State Key Laboratory of Genetic Engineering, School of Life Sciences, Fudan University, Shanghai 200438, China

2 School of Basic Medical Sciences, The First Affiliated Hospital of Nanchang University, Jiangxi Medical College, Nanchang University, Nanchang 330031, China

3 BMF Nano Material Technology Company Limited, Shenzhen 518017, China

4 Institute of Organoid Technology, Kunming Medical University, Kunming 650500, China

5 Shanghai American School, Shanghai 201100, China

6 Z Lab, bioGenous BIOTECH, Shanghai 200438, China

1 Introduction

Organoids are three-dimensional (3D) in vitro cellular constructs that recapitulate the key structural and functional aspects of organs [1–5]. While organoids can simulate certain aspects of real organs, they are limited by the absence of extracellular matrix components, immune cells, and functional vascular systems. This hinders the organoids' ability to replicate intricate organ functions in vivo, resulting in variations when assessing the organism's response to drugs [6, 7]. Currently, the combination of biomaterials and organoid technology using additive manufacturing techniques enables the rapid fabrication of 3D bioengineered structures for tissue engineering, such as vascular tissue models [8, 9]. Particularly, microfluidic organ-on-a-chip technology has become an increasingly attractive tool for both fundamental and practical research due to its significant advantages: high spatial resolution, high sensitivity, high integration, high controllability, and low costs [10–12].

The primary challenge in current tissue-engineered organ-on-a-chip technology is the cessation of cell proliferation and subsequent formation of a necrotic core once a specific size threshold is reached. The main cause of necrotic core formation is the size limitation of tissue-engineered grafts, due to limited diffusion of essential nutrients and gases in organoids larger than 400 μm [12, 13]. Furthermore, organ-on-a-chip technology faces significant obstacles in creating organ systems with capillary-like structures that accurately mimic the functionality of real microvascular networks because of 3D printing limitations in terms of resolution, material properties, and the ability to print complex geometries at small scales [7, 14].

To address the issue of nutrient supply in organ systems, recent research has focused on coculturing vascular endothelial cells or utilizing high-osmolarity hydrogels for 3D printing. These methods aim to produce an intricate network of microcapillaries to facilitate efficient substance transport and nutrient diffusion [15–17]. However, practical implementation poses several challenges, including the technical complexity of coculturing vascular cells and limitations in the structural strength and stability of prints using high-osmolarity hydrogels. These limitations hinder scalability and mass production [15]. Here, we used projection microstereolithography (PμSL) 3D printing to fabricate biocompatible organoids-on-a-chip for internal perfusion in organ-on-a-chip systems. PμSL is a rapid and flexible microscale 3D photopolymerization technique that combines an ultraviolet projection system with a digital dynamic mask and an *XYZ* motorized stage system. After projecting a cross-sectional image from the 3D computer-aided design model, it solidifies a layer of liquid photoreactive resin into the corresponding pattern. By repetitively stacking the new layer upon the previous one, it transforms the digital design into a complex 3D micro-structure. PμSL has both a high-resolution manufacturing capability by controlling the size of a pixel in a projection (up to 0.6 μm) and rapid production capability by producing one layer through one projection [18, 19].

Microfluidic technology exerts high control over cell culture conditions in various aspects, including the geometric configuration of culture devices and the fluid flow velocity, and can precisely control the volume of liquid. This can remarkably enhance the concentration of oxygen and glucose obtained by the culture [20]. Moreover, the microfluidic system can be automated to a large extent. The microfluidic cell culture system can culture cells for several weeks after resetting culture parameters (such as adding sufficient culture medium, setting the fluid velocity, and adjusting culture duration) without manual intervention [21]. Due to the above advantages—controllability, parallelization, automation, and excellent imaging characteristics, microfluidics has become particularly valuable for organoid culture. For designing the microfluidic chip, we followed three requirements: (1) Presence of an inlet supplying fresh culture medium into all vascular channels and another outlet to collect culture medium for analysis. (2) Exchanging culture media containing growth factors and other necessary proteins through vascular mimicking channels by narrow slits around the channel surface. The slit size allows for the passage of large molecular proteins while preventing cell access to perfusion channels. (3) The distance between neighboring channels and the distance between narrow slits around the channels are less or equal to the nutrients' diffusion limit (400 μm). A high-precision (2-μm resolution) 3D printing system, combined with a novel resin named BIO-1, was utilized to fabricate biocompatible chips featuring hollow channels. These channels possess an inner diameter of 80 μm, a wall thickness of 20 μm, and a spacing of 400 μm. Integrated evenly around the channels are four narrow slits with a width < 10 μm. Each group of slits was positioned at 300-μm intervals along the channels. Through these hollow channels and slits, it allows for perfusion into the internal compartment of the organoid culture system. Based on the combination of this engineered vascularized organoid-on-a-chip and microfluidic technology, we aim to break through the limitations caused by insufficient nutrient supply during the process of organoid culturing.

2 Materials and methods

2.1 Design of the organoid-on-a-chip and microfluidic platform

Organoids-on-a-chip were designed to have hollow tubes with an inner diameter of 80 μm, a wall thickness of 20 μm, and a channel spacing of 400 μm. Four slits were evenly placed

around the channels. The width of the narrow slits was < 10 μm. Each group of slits was spaced 300 μm apart along the tubes. The inlet and outlet each have a diameter of 0.75 mm. The 3D printing technology and BIO-1 were provided by BMF Precision Tech Inc. (Shenzhen, China), and the printer used was the microArch S230 (2-μm resolution).

2.2 Tissue collection and preparation

After collection, all lung cancer, endometrial cancer, airway, and kidney tissue specimens were preserved in a storage solution (primary tissue storage solution containing 1% penicillin-streptomycin; bioGenous, China) and transported to the laboratory. Tissue processing was completed within 1 d after extraction from the patient's body. Under sterile conditions, the minced tissue was placed in a fresh tissue digestion solution (bioGenous) and incubated at 37 °C for 60 min. Then, the digestion solution was agitated and filtered through a 100-μm cell strainer. After centrifugation, the supernatant was discarded and red blood cells were removed by incubating with red blood cell lysis solution (bioGenous) for 3 min. Single cells or cell aggregates were collected, washed three times in epithelial organoid basal medium (bioGenous), and cultured in a complete medium (bioGenous).

2.3 Culture of organoids and centimeter-scale tumoroids/organoids

First, established and stably cultured organoids (Day 7) were collected in phosphate-buffered saline (PBS). Then, they were digested in 1× organoid dissociation solution (bioGenous) at 37 °C for 5 min. The digested cells were then collected and washed three times with epithelial organoid basal medium. Next, cells were re-suspended in Matrigel to ensure a cell density >500,000 cells/mL. Subsequently, 30 μL of the cell suspension was added to the bottom of the organoid-on-a-chip and allowed to solidify for 15 min at 37 ℃, followed by the addition of 70 μL of cell suspension following the same procedure. The organoid-on-a-chip was then mounted onto a microfluidic device, and the program was initiated after adding a complete medium (bioGenous). The flow rate was set to <2 μL/min.

2.4 Immunofluorescence and hematoxylin and eosin (H&E) staining

Before immunofluorescence (IF) staining, the post-cultured centimeter-scale tumoroids/organoids were first detached from the microfluidic device, and a cover glass was tightly adhered to the bottom of the chip to prevent leakage of the co-cultured fluids. Subsequently, the centimeter-scale tumoroids/organoids were fixed in 500 μL of 4% paraformaldehyde and incubated at 4 °C for 30 min. Then, 3% (0.03 g/mL) melted and heated agar was poured into the tumoroids/organoids. After the agar cooled down, it was dehydrated, embedded, and sectioned. After dewaxing, the slides were then washed with PBS and permeabilized using 0.25% Triton X-100 in PBS for 30 min. Next, centimeter-scale tumoroids/organoids were washed with PBST (PBS containing 0.1% Tween 20) and blocked with 5% bovine serum albumin (BSA) for 1 h, before incubation with primary antibodies at 4 °C overnight, followed by three washes with PBST. Subsequently, the centimeter-scale tumoroids/organoids were incubated with secondary antibodies and Hoechst at room temperature, protected from light, for 1 h (all antibodies are shown in Table S1 in the supplementary information). Finally, the organoids were imaged using a confocal microscope (DMI8, Leica).

After deparaffinization and rehydration, the slides were stained with H&E, dehydrated, and mounted. Images were acquired with a Leica DM6B upright microscope.

2.5 RNA sequencing

The total RNA of centimeter-scale tumoroids/organoids was isolated using the RNAprep Pure Micro Kit (Tiangen) and sent to Novogene for quality control and sequencing, before library establishment for transcriptome analysis using the Applied Biosystems SOLiD^{TM} Sequencing platform. Differentially expressed genes (DEGs) were obtained with a false discovery rate (FDR) <0.1 and a fold variation >2. The enriched signaling pathways in DEGs were determined through gene set enrichment analysis using the Pathway Interaction Database [22] and Gene Set Enrichment Analysis (GSEA) v2.0.14 [23].

2.6 Recombinant adeno-associated virus (AAV) vector production

Highly purified stocks of recombinant AAV vectors were generated through triple-plasmid transfection, following a previously described method [24]. In brief, HEK293 cells were co-transfected with three plasmids using polyethyleneimine (Polysciences) as per manufacturer's instructions. After 72 h of transfection, cells were collected and subjected to three freeze-thaw cycles. Subsequently, cells were digested with 50 U/mL of Benzonase (Merck). For purification of viral vectors, iodixanol (Sigma-Aldrich) gradient ultracentrifugation was performed, followed by ion exchange chromatography with HiTrap SP/Q HP columns (GE Healthcare). The purified vectors were then washed with PBS and concentrated using centrifugal spin concentrators with a 150,000 molecular weight cutoff (Merck). Finally, the physical genomic titer of recombinant vector stocks was measured using quantitative reverse transcription polymerase chain reaction (RT-PCR).

2.7 Cell proliferation assay

The growth rate of organoids was measured as described previously [25]. Briefly, cells were seeded in an organoid-on-a-chip. At 0, 48, 96, 144, and 192 h after drug exposure, the LiveCell-Fluo^{TM} Organoid Vitality Assay Kit (bioGenous) (buffer A:B=10:1) was used for cell viability detection. The working solution was prepared according to the instructions, with buffer A and buffer B mixed at 10: 1, and the cells were incubated at 37 °C for 2 h. Then, the absorbance at 450 nm was measured in a microplate reader.

In addition, after organoid amplification, bright-field images of different growth stages were collected using BioTek Cytation 7 (Agilent), and the area of the organoids was calculated using ImageJ software.

2.8 Statistical analysis

The experimental results were analyzed using *t*-tests or one-way analysis of variance (ANOVA). All *p*-values were two-sided, and considering multiple testing, significance was only considered for $p<0.01$. All statistical tests were performed using Prism (GraphPad Software, USA) and Microsoft Excel. Unless otherwise noted, mean±standard error of the mean (SEM) is shown in all plots. A 95% confidence interval was used to determine significance ($p<0.05$). All sample sizes and *p*-values are reported in figures or figure legends.

3 Results

3.1 Microvascular capillary organoid-on-a-chip based on 3D precision printing

To simulate a more physiologically relevant capillary network, a capillary organoid-on-a-chip was developed through high-precision 3D printing. Specifically, we designed printed "vessels" that consist of hollow tubes (Fig. 1a; Fig. S1a in the supplementary information). To replicate the gradual dispersion of nutrients from the vascular network, small holes with a diameter of 7–10 μm were printed on the channel walls (Figs. 1b and 1c; Fig. S1b in the supplementary information). Further, to mimic a network of intersecting blood vessels in a capillary organoid-on-a-chip, five layers of such vascular networks were printed, each comprising 14 printed "vessels" with seven additional crossbars for stabilization and support of the vascular network (Figs. 1a and 1b; Fig. S1a in the supplementary information). In addition, to evaluate the biocompatibility of the BIO-1 resin used for manufacturing the capillary organoid-on-a-chip, we co-cultured various types of organoids using the soaking solution of the BIO-1 resin. The BIO-1 resin did not have any adverse effects on organoid expansion (Figs. S1d and S1e in the supplementary information). Furthermore, different concentrations of the soaking solution of the BIO-1 resin had no adverse effects on the activity of organoids derived from human lung cancer (tumor source) and from the airway and kidney (normal tissue source) (Fig. S1f in the supplementary information).

A perfused vascularized model aims to simulate the dynamic characteristics of blood flow by employing a pulse pump and utilizing gravity or capillary effects [26]. The movement of fluids in such a device generates shear stress on the blood vessel walls, which is an important regulator of permeability [27]. To mimic blood flow dynamics in the body, we designed an infusion device (Fig. 1d). Specifically, the culture medium was slowly injected into the chip at 2 μL/min using an injection pump. The fluid rapidly permeated throughout the device through the small holes on the channels, while the system enabled fluid flow circulation, effectively simulating the characteristics of micro-arteries and micro-veins in the body (Fig. 1d; Fig. S1c and Video S1 in the supplementary information). Meanwhile, we designed an "organoid-on-a-chip platform" for capillary organoid-on-a-chip. This device consists of a base or holder to accommodate the organoid-on-a-chip, as well as a cover on top. To prevent culture medium leakage, a polydimethylsiloxane (PDMS) coating was incorporated (Figs. 1d–1f).

3.2 Establishment of a lung cancer centimeter-scale tumoroid

We first constructed a patient-derived lung cancer organoid (Fig. 2a). These lung cancer organoids typically cease to increase in size after approximately 7 d and remain within a diameter of 200 μm (Fig. 2b). To facilitate organoid cultivation in a chip, we introduced digested lung cancer organoids into a Matrigel mixture and inoculated them into a capillary organoid-on-a-chip. By following the protocol outlined in Fig. 1c and Fig. S1c (supplementary information), digested organoid fragments were successfully transplanted into a capillary organoid-on-a-chip, and sustained growth was observed for >30 d (Fig. 2c; Fig. S2a in the supplementary information). Due to the remarkable capacity of these tumor cultures to support long-term and large-scale cultivation of cancer organoids, as well as their unique growth characteristics and structural features, we refer to this in vitro model as "centimeter-scale tumoroids" (Figs. 2a and 2c). Similarly, Ki67 staining showed that lung cancer centimeter-scale tumoroids exhibited higher proliferative activity than lung cancer organoids (Fig. 2d).

Additionally, immunostaining of these organoids and centimeter-scale tumoroids showed that the centimeter-scale tumoroids displayed histopathological and molecular characteristics matching those of the tumor tissues they derived from (Fig. 2e). In addition, IF staining with thyroid transcription factor 1 (TTF-1) and NapsinA antibodies confirmed their lung cancer origin (Fig. 2f). These data indicated that

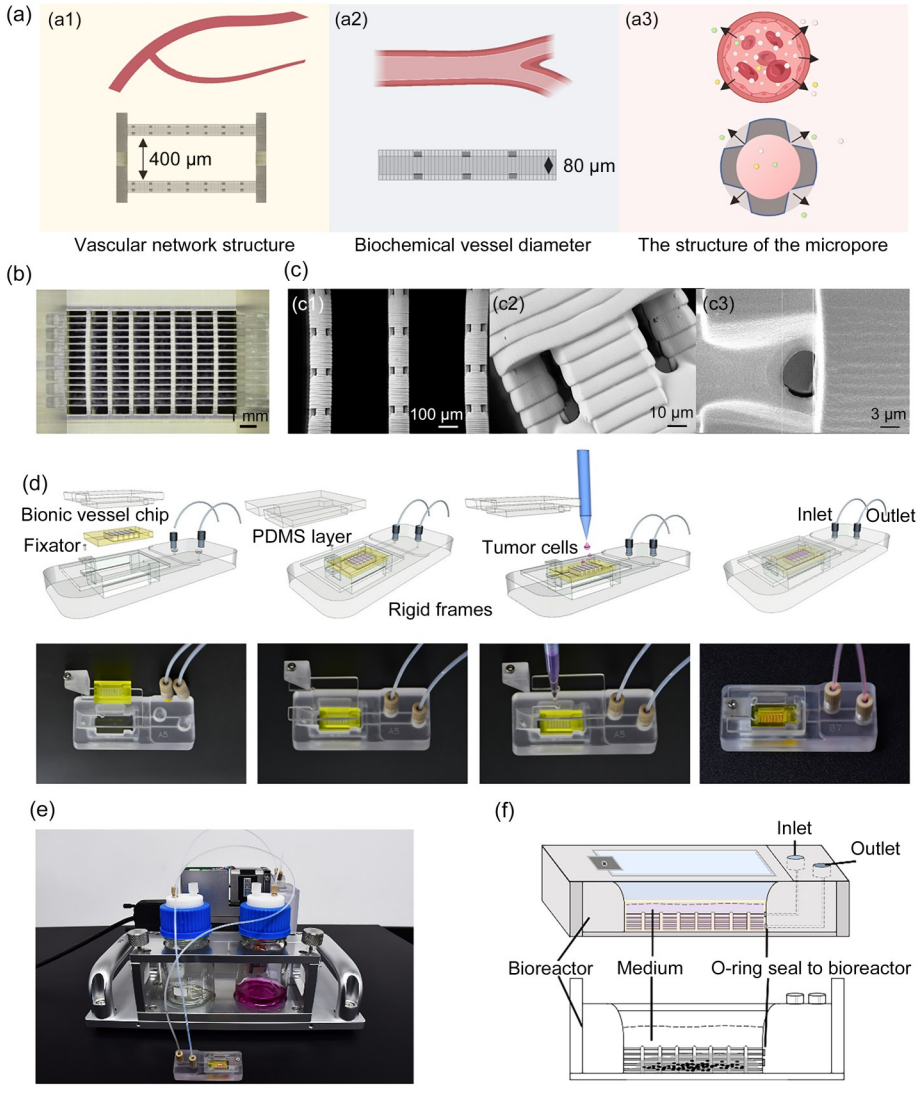

Fig. 1 Fabrication of a vascularized organoid-on-a-chip using micro-3D printing. (a) Cross-sectional illustrations of the engineered microvascular networks in the organoid-on-a-chip: (a1) distance of the engineered vessel (400 μm); (a2) biochemical vessel diameter (inner diameter: 80 μm; outer diameter: 120 μm); (a3) micropore diameter (7 μm). (b) A 3D-printed organoid-on-a-chip designed with microfluidic capillary grids. (c) TEM images of the hollow tubes (c1) and holes (c2, c3) in capillary organoids-on-a-chip. (d) Schematic illustrating the design principles and assembly process of the device (top row); device components and assembly process (bottom row). (e) An example of a microfluidic device. The 3D-printed organoid-on-a-chip was adapted with permission from BMF Precision Tech Inc. (f) Position of the organoids-on-a-chip within the platform and introduction of a 1:1 mixture of 1,000,000 cells and 30 μL Matrigel. TEM: transmission electron microscopy

the centimeter-scale tumoroids might serve as an important supplement to organoids in terms of simulating lung cancer, especially in case of potential size requirement.

Remarkably, the organoids grew within the chip beyond previous size limitations (<400 μm), as shown in Fig. 2g. During conventional cultivation, lung cancer organoids, which originate from epithelial cells, tend to form vesicle-like structures that resemble the arrangement of the epithelial cells in the body. However, due to the restricted availability of nutrients, these cells can only grow by enlarging the vesicular structure until a significant number of cells undergo apoptosis (Fig. S2b in the supplementary information), ultimately limiting their long-term survival and growth. In the capillary organoid-on-a-chip, organoid growth in the chip can be divided into three stages. Initially, after digestion and transplantation into the chip, organoids formed spherical structures. During cultivation, these small organoid spheres gradually increased in size, resembling the growth in traditional organoid cultures. However, with extended cultivation time, these organoid spheres behaved differently, as they continued to grow without undergoing disintegration of organoid structures and cellular apoptosis (Fig. 2g). After 12 d of culture, these organoids established tight connections and formed a whole entity, resembling in vivo tumors with vascular structures (Figs. 2g and 2h; Figs. S2a and S2c in the supplementary information).

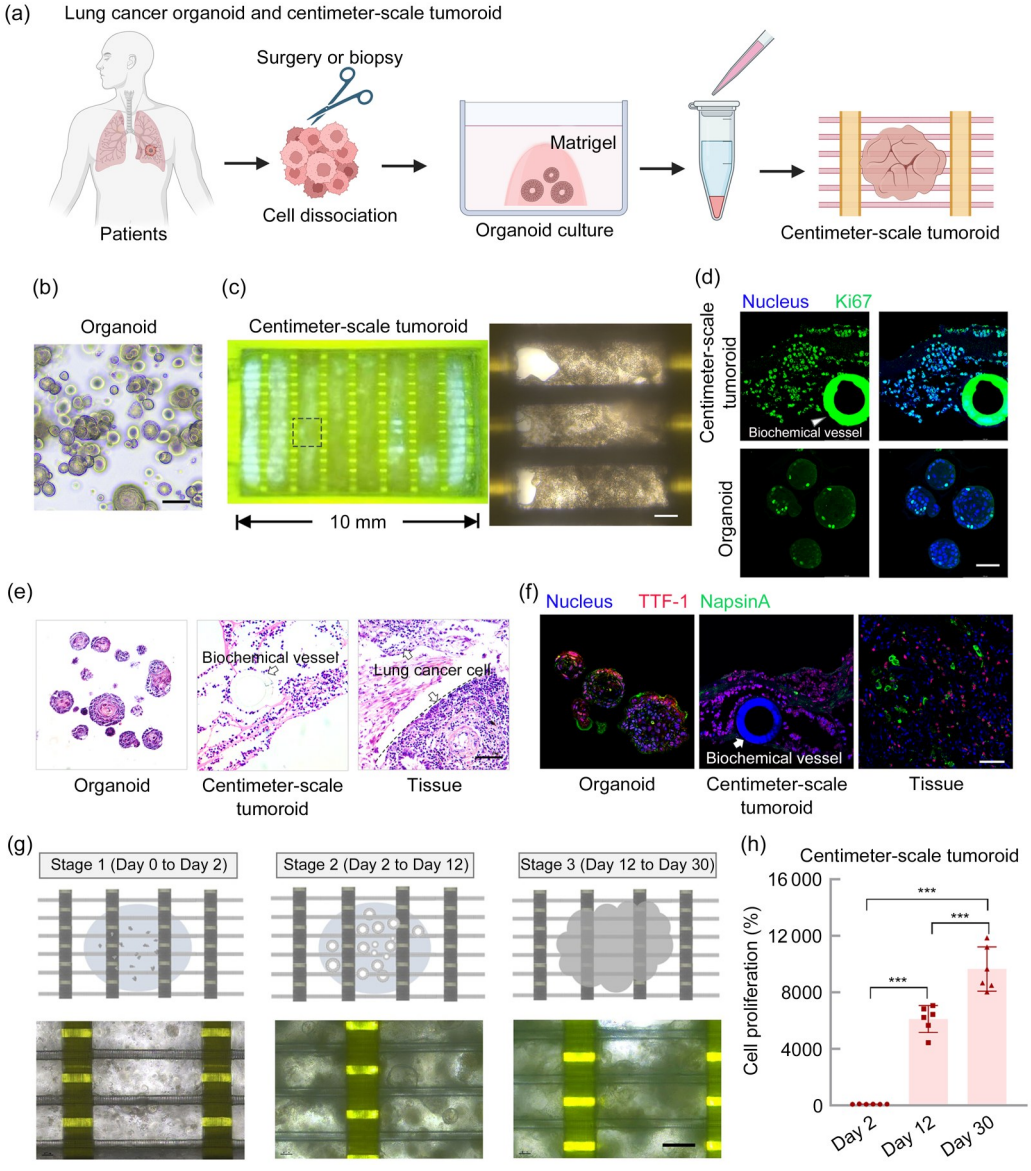

Fig. 2 Establishment of organoids for lung cancer. (a) Diagram of the development of lung cancer organoids from patient tumors for long-term culture. Created in BioRender (https://BioRender.com/f10h891). (b) Bright-field images of lung cancer organoids in Matrigel on Day 7 (scale bar: 100 μm). (c) Image of lung cancer (centimeter-scale) tumoroids cultured on the chip, with cells covering almost the entire chip surface after 30 d of cultivation. (d) Immunofluorescent staining images of centimeter-scale tumoroids (Ki67 (green) for cell proliferation detection; scale bar: 50 μm). (e) H&E staining images of lung cancer organoids, centimeter-scale tumoroids, and tissues (scale bar: 50 μm). (f) Immunofluorescent staining images of organoids, centimeter-scale tumors, and tissues. Lung cancer organoids and centimeter-scale tumoroids retained the tumor cell organization and expression patterns of characteristic markers (TTF-1 (red) and NapsinA (green) for lung cancer; scale bar: 50 μm). (g) Images of centimeter-scale lung cancer cultured on the organoid-on-a-chip were obtained, demonstrating the continuous growth of the centimeter-scale lung cancer from Day 0 to Day 30. The formation process of centimeter-scale tumoroids can be categorized into three stages (scale bar: 200 μm). (h) Bar graph showing cell expansion changes from 2 to 30 d. Data are expressed as mean±standard deviation (n=6, $^{***}p$<0.001)

3.3 Lung cancer centimeter-scale tumoroids demonstrate heightened sensitivity to cisplatin exposure

Cisplatin is a chemotherapy drug used in the clinical treatment of non-small-cell lung cancer for patients not eligible for surgical resection [18, 28] and is commonly used as a principal chemotherapy drug for small-cell lung cancer. To assess the sensitivity of these large-scale centimeter-scale tumoroids to anticancer drugs, we initially examined the responsiveness of a conventional organoid to cisplatin. The results indicated that a half maximal inhibitory concentration (IC_{50}) of lung cancer organoid is 29.88 μmol/L (Fig. 3a). Subsequently, we used 10 μmol/L cisplatin to conduct drug sensitivity testing on lung cancer centimeter-scale tumoroids. Substantial tumor cell death was observed after 5 d of drug exposure

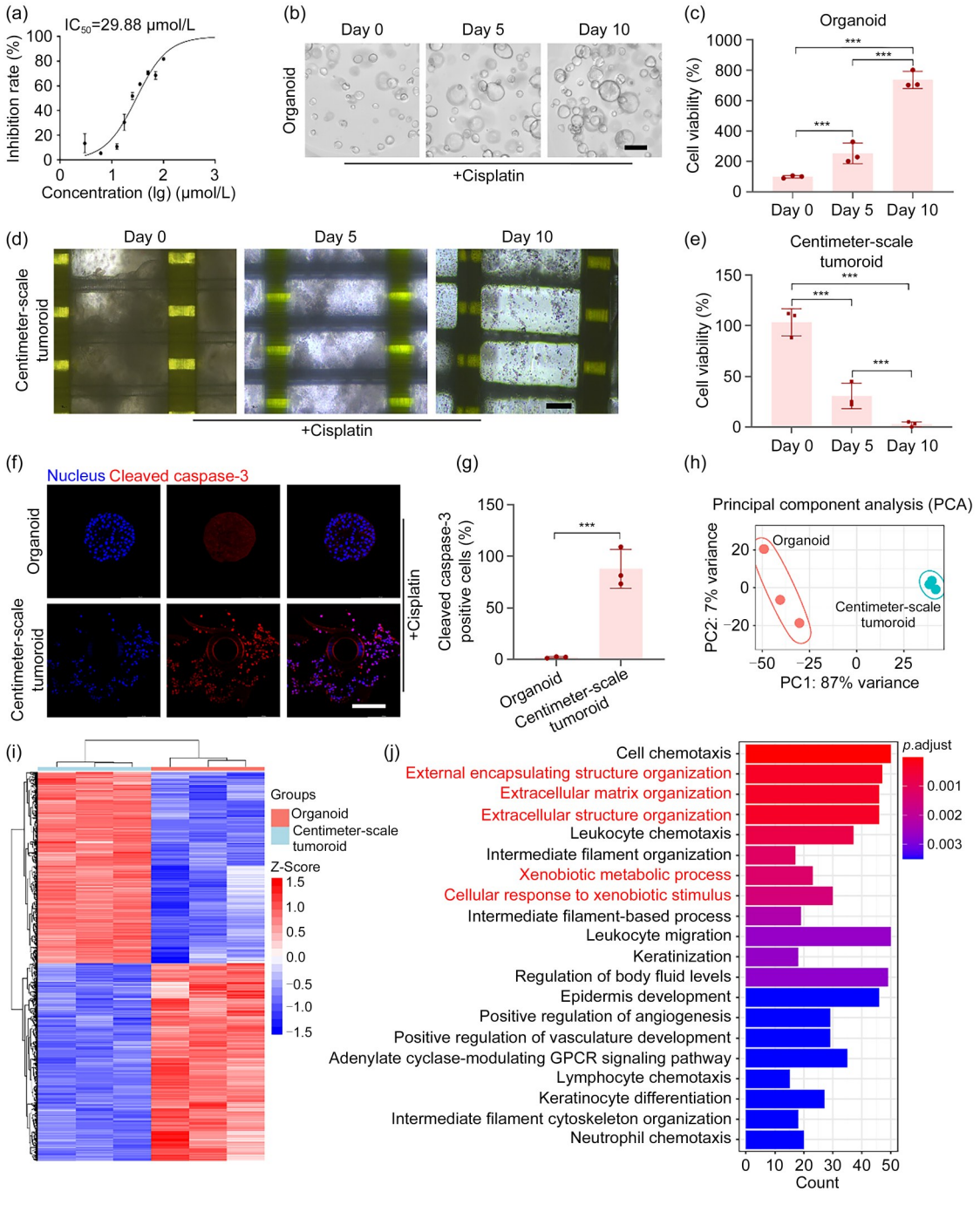

Fig. 3 3D-printed centimeter-scale tumoroid chip. (a) Overlapped fitted dose-response curves of the lung cancer organoid-cisplatin measured in the microplate (off-chip) (n=3 biologically independent samples; data are presented as mean±standard deviation). (b) A representative example illustrating changes in the lung cancer organoids from 0 to 10 d after stimulation with 10 μmol/L cisplatin (n=3 biologically independent lung cancer organoids in the right panel; scale bar: 200 μm). (c) Bar graph showing cell expansion changes in the lung cancer organoid from 0 to 10 d after stimulation with 10 μmol/L cisplatin (n=3, $^{***}p$<0.001). (d) A representative example (centimeter-scale tumoroid) illustrating the differences between on-chip drug sensitivity of the centimeter-scale tumoroids and those of the organoids (n=3 biologically independent lung cancer organoids in the right panel; data presented as mean±standard deviation; scale bar: 200 μm). (e) Bar graph showing changes in cell expansion in lung cancer centimeter-scale tumoroids from Day 0 to Day 10 after stimulation with 10 μmol/L cisplatin (n=3, $^{***}p$<0.001). (f) Immunofluorescent staining images of lung cancer organoids and centimeter-scale tumoroids. Cleaved caspase-3 (red) represents apoptotic cells; scale bar: 100 μm). (g) Bar graph showing the proportion of cleaved caspase-3-positive cells in lung cancer organoids and centimeter-scale tumoroids (n=3, $^{***}p$<0.001). (h) Principal component analysis of three samples. (i) Heat map showing the DEGs in lung cancer centimeter-scale tumoroids compared to control lung cancer organoids after stimulation with cisplatin. (j) Top 20 signaling pathways in lung cancer centimeter-scale tumoroids compared with the control lung cancer organoids after 6 d of stimulation with 5 μmol/L cisplatin based on GO analysis. Data in (c, e, g) are expressed as mean±standard deviation. GO: gene ontology

(Figs. 3d and 3e). After 10 d 10 μmol/L cisplatin-exposure, cells were completely eradicated in lung cancer centimeter-scale tumoroids. However, exposure to 10 μmol/L cisplatin had no significant effect on the lung cancer organoid model (Figs. 3b and 3c). We performed immunofluorescence imaging of drug-treated organoids and lung cancer centimeter-scale tumoroids. At the same concentration, cisplatin induced more apoptosis of lung cancer cells in centimeter-scale tumoroids than in organoids (Figs. 3f and 3g). These results demonstrated the higher sensitivity of lung cancer centimeter-scale tumoroids to cisplatin.

To investigate the underlying mechanisms of cisplatin's effects on centimeter-scale tumoroids, overall genome transcriptome analysis was performed on lung cancer centimeter-scale tumoroids and lung cancer organoids after stimulation with cisplatin (Figs. 3h–3j). The heat map in Fig. 3i shows 929 up-regulated and 1420 down-regulated genes in lung cancer centimeter-scale tumoroids compared to control lung cancer organoids. Next, we analyzed signaling changes in lung cancer organoids based on gene ontology (GO) enrichment analysis. Interestingly, cell chemotaxis, external encapsulating structure organization, extracellular matrix organization, and extracellular structure organization were most significantly active in lung cancer centimeter-scale tumoroids (Fig. 3j). We also observed that DNA damage-related pathways were the most enriched signaling pathway in lung cancer centimeter-scale tumoroids after cisplatin stimulation (Fig. S3 in the supplementary information). The different drug sensitivities of lung cancer centimeter-scale tumoroids and organoids to cisplatin are attributed to the different dependencies on the extracellular matrix after the cultivation of the two different-sized models, as well as differences in the tissue structure and metabolic pathways.

3.4 Establishment of a centimeter-scale tumoroid of endometrial cancer and drug sensitivity testing

To better replicate the microphysiological systems of the human endometrium, microfluidic technology could offer ease-of-use, optical transparency, and oxygen permeability [29], but these models still lack a vascular system for nutrient delivery [30, 31]. To faithfully replicate the microenvironment of endometrial cancer and characterize the response of centimeter-scale tumoroids to drugs, we developed an in vitro model that mimics the microenvironment of endometrial cancer. First, patient-derived cancer cells were used to cultivate organoids resembling endometrial cancer tissue. Then, the vascular network in the endometrium was simulated to supply nutrients and oxygen to the spheroids via an organoid-on-a-chip (Fig. 4a) and introduced a microfluidic system to simulate the blood circulation in the endometrium.

After a long cultivation period (over 15 d), these endometrial cancer organoids gradually established connections, forming histologically cohesive structures that closely resembled the tumor in vivo (Figs. 4b and 4c). In contrast, unperfused organoids ceased to grow and began to disintegrate (Figs. S4a and S4b in the supplementary information). In addition, pathological staining showed that all endometrial cancer organoids displayed histopathological and molecular characteristics matching those of the tumor tissues they derived from (Fig. S4c in the supplementary information). IF staining with progesterone receptor (PR), estrogen receptor (ER), and cytokeratin 7 (CK7) antibodies confirmed their endometrial cancer origin (Figs. 4d and 4e).

Carboplatin is a common anticancer drug used in the treatment of endometrial cancer. However, endometrial cancer organoids are not sensitive to carboplatin (Figs. 4f–4h), inconsistent with clinical observations. Subsequently, endometrial cancer tumoroids were subjected to antitumor drug testing (Figs. 4i and 4j). Tumoroids displayed a much more sensitive response to the drug compared with classical endometrial cancer organoids under the same carboplatin concentration (Figs. 4g–4j; Fig. S4d in the supplementary information).

In addition, this endometrial cancer centimeter-scale tumoroid platform can be used for long-term monitoring of the response of the same tumor to different drug concentrations, thereby capturing therapeutic adaptation outcomes following prolonged clinical treatment. As shown in Fig. 4k, endometrial cancer centimeter-scale tumoroid cells rapidly died with increasing carboplatin concentrations. These results indicate that the endometrial cancer centimeter-scale tumoroid culture platform not only provides a better simulation of the growth microenvironment of endometrial cancer, achieving breakthroughs in tumoroid growth scale, but also allows for a more accurate evaluation of drug efficacy.

3.5 Centimeter-scale kidney organoid culture and nephrotoxicity testing

Next, we applied our capillary organoid-on-a-chip method to kidney organoids (Figs. 5a–5d). HE staining of these centimeter-scale kidney organoid models showed histological characteristics matching those of the kidney tissues they derived from (Fig. 5e). Moreover, IF staining showed expression of the distal tubule marker low-density lipoprotein receptor-related protein 2 (LRP2) and the distal tubule of the kidney marker E-cadherin (ECAD) (Figs. 5f and 5g).

To assess the nephrotoxic effects of cisplatin in a biologically relevant and dynamic setting, centimeter-scale kidney organoids were labeled with green fluorescent protein (GFP) for long-term survival and evaluation of cell proliferation (Fig. 5h). We then subjected our centimeter-scale kidney organoids cultured for 30 d to cisplatin treatment. After 4 d of culture, kidney cells began to exhibit signs of cell death,

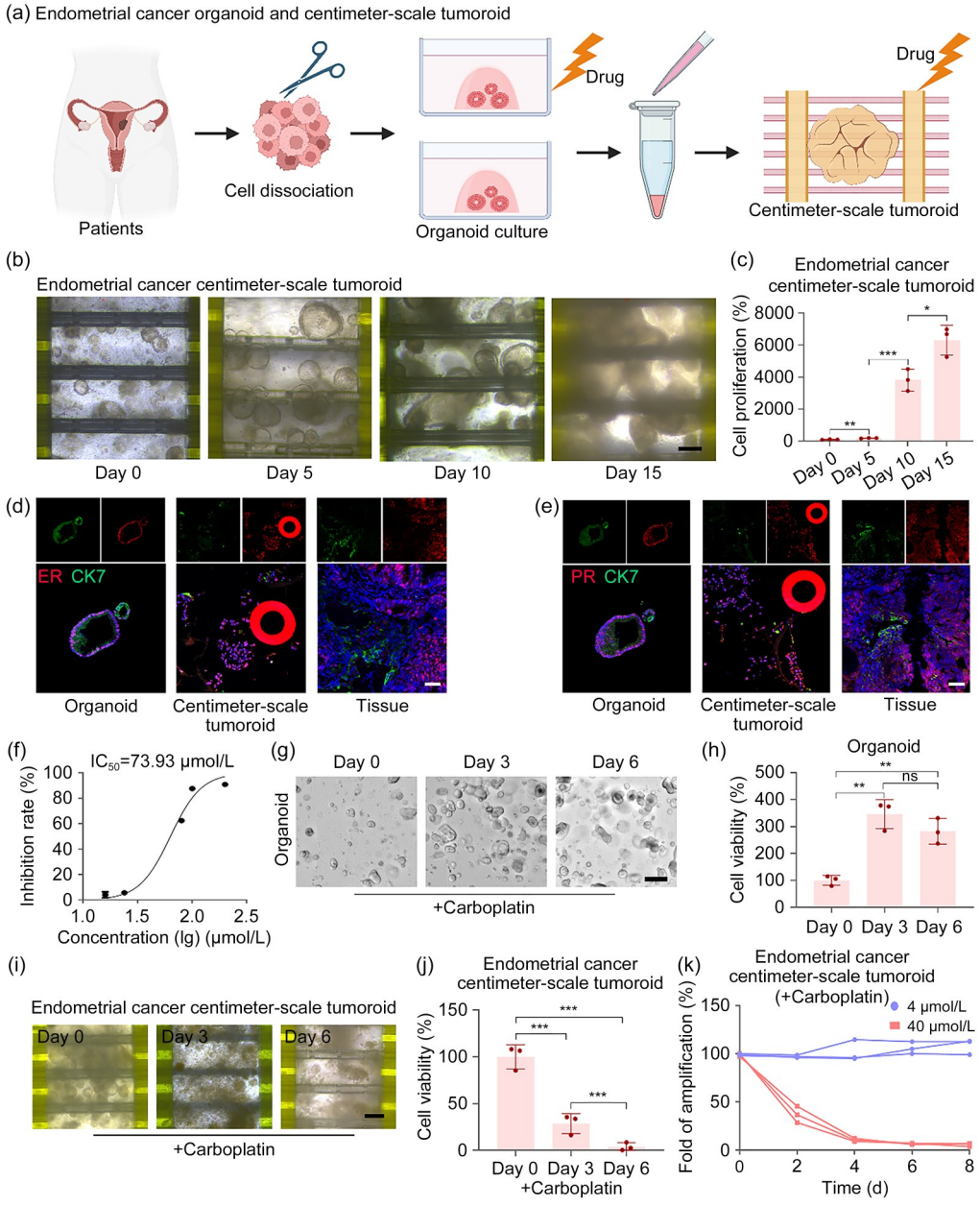

Fig. 4 The one-week drug sensitivity test performed on the organoid-on-a-chip. (a) Diagram of the process of establishing endometrial cancer organoids from patient tumors for the subsequent centimeter-scale tumoroid culture and drug screening. Created in BioRender (https://BioRender.com/f10h891). (b) Images of endometrial cancer organoid cultured on the organoid-on-a-chip, showing the continuous growth of endometrial cancer organoid from Day 0 to Day 15 (scale bar: 200 μm). The experiments were repeated three times. (c) Bar graph showing the cell expansion fold of endometrial cancer centimeter-scale tumoroid varied from Day 0 to Day 15 (n=3, $^{**}p< 0.01$, $^{***}p<0.001$). (d) Immunofluorescent staining images of organoids, centimeter-scale tumoroids, and tissues. The endometrial cancer organoids and centimeter-scale tumoroids retained the tumor cell organization and the expression patterns of the characteristic markers (ER (red) and CK7 (green) for endometrial cancer; scale bar: 50 μm). (e) Immunofluorescent staining images of organoids, centimeter-scale tumoroids, and tissues. The endometrial cancer organoids and centimeter-scale tumoroids retained the tumor cell organization and the expression patterns of the characteristic markers (PR (red) and CK7 (green) for endometrial cancer; scale bar: 50 μm). (f) Overlapped fitted dose-response curves of endometrial cancer organoid-carboplatin measured in the microplate (off-chip) (n=3 biologically independent cells, data are presented as mean±standard deviation). (g) A representative example illustrating that the endometrial cancer organoid varied from 0 to 6 d after stimulation with 40 μmol/L carboplatin (scale bar: 200 μm). (h) Bar graph showing the cell expansion fold of the endometrial cancer organoid varied from 0 to 6 d after stimulation with 40 μmol/L carboplatin (n=3, $^{**}p<0.01$; ns: not significant). (i) A representative example (centimeter-scale tumoroid) illustrating that the on-chip drug sensitivity results of the centimeter-scale tumoroid were not in agreement with the responses of the organoids (scale bar: 200 μm). (j) Bar graph showing the cell expansion fold of endometrial cancer centimeter-scale tumoroid varied from 0 to 6 d of stimulation with 40 μmol/L carboplatin (n=3, $^{***}p<0.001$). (k) Survival curves of centimeter-scale tumoroid stimulated with 4 and 40 μmol/L carboplatin for 8 d (n=3 biologically independent endometrial cancer centimeter-scale tumoroids). Data in (c, h, j) are expressed as mean±standard deviation

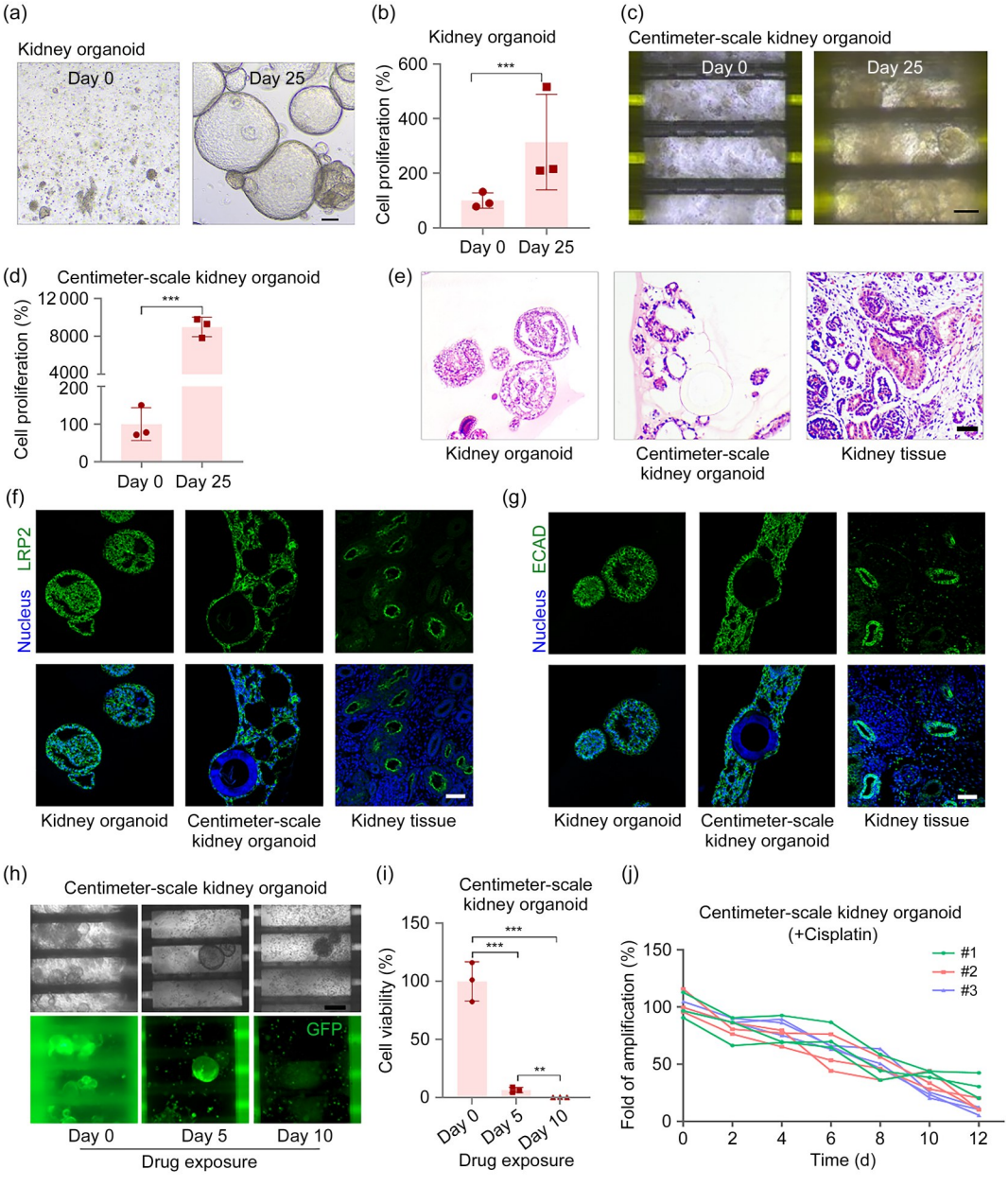

Fig. 5 Culture of kidney organoids and detection of nephrotoxicity. (a) Bright-field images of kidney organoids at Days 0 and 25 post-seeding in Matrigel (scale bar: 100 μm). (b) Bar graph showing the cell expansion fold of kidney organoids over 2 to 25 d (n=3, $^{***}p$<0.001). (c) Images of centimeter-scale kidney organoids cultured on the organoid-on-a-chip, showing the continuous growth of kidney organoids from Days 0 to 25 (scale bar: 200 μm; n=3). (d) Bar graph showing the cell expansion fold of centimeter-scale kidney organoids varied from 2 to 25 d (n=3, $^{***}p$< 0.001). (e) H&E staining images of kidney organoids, centimeter-scale organoids, and tissues (scale bar: 50 μm). (f) Immunofluorescent staining of LRP2 (green) images of kidney organoids (scale bar: 50 μm; n=3). (g) Immunofluorescent staining of E-cadherin (green) images of kidney organoids (scale bar: 50 μm; n=3). (h) A representative example (centimeter-scale kidney organoid) illustrating that the on-chip drug sensitivity results of the centimeter-scale kidney organoids were not in agreement with the responses of the organoid (n=3 biologically independent kidney organoids in the right panel, data are presented as mean±standard deviation). (i) Bar graph showing the cell expansion fold from Day 0 to Day 10 of stimulation with 5 μmol/L cisplatin (n=3, $^{**}p$<0.01, $^{***}p$<0.001). (j) Survival curves of the centimeter-scale kidney organoid stimulated with 5 μmol/L cisplatin for 12 d (n=3 biologically independent samples). Data in (b, d, i) are expressed as mean±standard deviation

leading to organoid disintegration and the development of vesicle-like structures, mirroring the characteristic dilation of the proximal renal tubules exposed to cisplatin [32] (Figs. 5h and 5i; Video S2 in the supplementary information). When exposed to the drug for >10 d, >50% of cells died (Fig. 5j). These results suggest that the capillary organoid-on-a-chip method is effective in culturing centimeter-scale kidney organoids with similar histological and molecular characteristics to native kidney tissues, which can effectively recapitulate the nephrotoxic responses to cisplatin.

3.6 Microvascular capillaries enable efficient gene delivery to centimeter-scale tumoroids

Although organoids serve as highly biomimetic models, the presence of extracellular matrix gels, such as Matrigel, creates a barrier that hinders direct viral infection, posing challenges to the development of recombinant adeno-associated viral vector (rAAV) gene therapies. To mimic the sensitivity of vascularized tumoroids or organoids to viral infection in the body, we utilized a fluidic system for rAAV-GFP delivery and evaluated the efficiency of infection (Figs. 6a and 6b). Through microfluidics, we injected fresh rAAV-GFP into centimeter-scale tumoroids, allowing the rAAV-GFP to slowly enter and fully react with the cells. After continuous infection for 48 h, we detected the infection efficiency of tumoroids based on the ratio of GFP^+ cells. Compared with organoids, centimeter-scale tumoroids showed more GFP^+ cells and a higher fluorescence ratio (Figs. 6c and 6d), indicating that the vascularized device significantly enhanced virus infectivity in centimeter-scale tumoroids (Fig. 6e), and these tumoroids maintained good proliferation activity. Overall, this platform for the development of rAAV therapy based on centimeter-scale tumoroids has the potential to advance the field of gene therapy and improve patient outcomes.

4 Discussion

This study demonstrates the use of PμSL 3D printing technology to fabricate biochips for organoid-on-a-chip applications which mimic the structure of microvascular networks as closely as possible and better simulate the processes of blood circulation and the exchange of crucial nutrients, oxygen, and metabolic waste removal. Our microfluidic channels boast a V-shaped design, which, in conjunction with hydrogel barriers, prevents cell backflow into the channels while facilitating the flow of growth factors, amino acids, and glucose. These hydrogels act as both an extracellular matrix substitute and a buffer for the rigid resin materials utilized for blood vessel printing, which allow for stable cell positioning and the ideal microenvironment for optimal growth. Using this cultivation system, we successfully developed large-scale cultures of tumor and normal tissues, enabling us to evaluate their response to drugs and assess their toxic effects. For the first time, we have successfully accomplished the precise printing of microvascular networks within organoid-on-a-chip, and the diameters of these engineered microvessels are highly proximate to those of the minute blood vessels of the body. Furthermore, we have verified that this type of organoid-on-a-chip exhibits remarkable biocompatibility. Through the employment of a microfluidic platform for

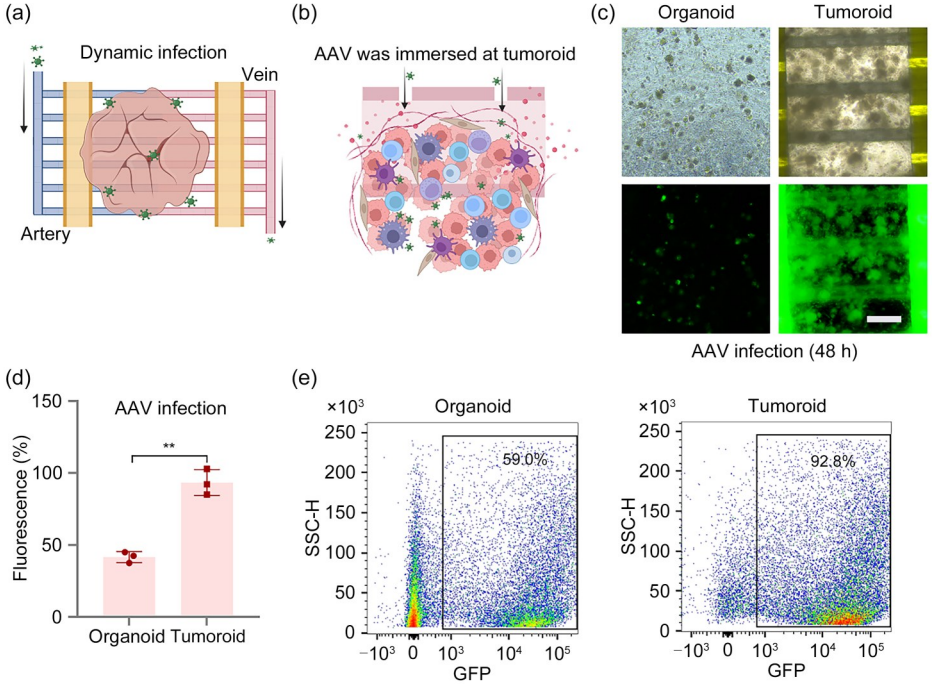

Fig. 6 Delivery of adeno-associated virus to centimeter-scale tumoroids by microvascular capillaries. (a) AAV is recirculated into a centimeter-scale tumoroid by fluid flow. (b) AAV and cells were in full contact through infiltration. Created in BioRender (https://BioRender. com/f10h891). (c) The lung cancer centimeter-scale tumoroid and organoids were infected with AAV for 48 h. GFP represents organoids that have been transfected (scale bar: 200 μm). (d) The lung cancer centimeter-scale tumoroids and organoids were infected with AAV for 48 h. The fluorescent areas were counted separately. The experiments were repeated three times. (e) Flow cytometry of lung cancer cells showed the gate and frequency of GFP^+ from lung cancer centimeter-scale tumoroids and organoids at 48 h following AAV treatment (n=3). Data in (d) are expressed as mean±standard deviation

culturing organoid-on-a-chip, we enabled cancer organoids and kidney organoids to be cultured for a duration of 30 d, and these cultures could expand to a centimeter scale. This overcomes the size constraints of traditional organoids. The centimeter-scale tumoroids and organoids offer an outstanding evaluation platform for drug and toxicological evaluations.

In this study, the flexibility and branching structure of the vasculature are still limited by the inherent constraints of the resin-based materials that are currently employed for printing. This limitation significantly hampers the chip's ability to accurately replicate and simulate the complex physical properties of the blood vessel walls. The resin materials lack the necessary pliability and intricate branching capabilities required to mimic the real-life vascular architecture precisely. Furthermore, in the context of organ-on-a-chip research, understanding and constructing accurate models of the crosstalk among epithelial cells, endothelial cells, and immune cells poses a crucial and formidable challenge that demands extensive further exploration. The interactions between these cell types are highly intricate and dynamic, involving a multitude of signaling pathways and molecular mechanisms. Adequately representing and studying these crosstalk processes within the confined environment of a chip is essential for developing more physiologically relevant and accurate organ models, but significant obstacles remain in achieving this goal.

Our research holds significant implications for the prospective advancement of organoid-on-a-chip. Precisely, 3D printing of engineered microvessels has been successfully accomplished within this study. Additionally, this particular type of organoid-on-a-chip is conducive to large-scale manufacturing, thereby facilitating the transformation of organoid chips from the laboratory setting to the industrial production line in the forthcoming era. On the chip, we developed a stable 3D-printed organoid-on-a-chip that can be used to cultivate for long periods on a large scale through perfusion with culture media. Our developed "centimeter-scale organoid" showed a larger scale, higher similarity to tissues, and a longer culture time. In the vascularized organoid-on-a-chip, the organoid culture reached a centimeter scale, exhibited a different morphology from that of organoids, and could be continuously cultured for more than 30 d. Further, these centimeter-scale organoids display different sensitivity to drugs and viral infection than traditional organoid cultures. This innovative approach, which employs a vascularized centimeter-scale organoid, represents a breakthrough in organ cultivation techniques, overcoming the limitations imposed by nutrient permeation, allowing for culture media circulation to quickly remove harmful metabolic waste and promoting long-term cell survival. This new, more biomimetic organoid-on-a-chip cultivation model holds promise as an in vitro drug screening platform for personalized therapy.

Supplementary Information The online version contains supplementary material available at https://doi.org/10.1631/bdm.2400424.

Acknowledgements This work was supported by the National Key Research and Development Program of China (No. 2024YFA1300128), the National Natural Science Foundation of China (No. 82372663), the Key Research and Development Program of Yunnan Province (No. 202302AA310024), the Key Research and Development Program of Jiangxi Province (No. 20232BBG70024), and the Natural Science Foundation of Shandong Province (No. ZR2023LSW008).

Author contributions Conceptualization, XFG, CY, and BZ; methodology, XFG and CY; investigation, XFG, CY, JCP, XD, HY, AGW, and EED; writing—original draft, XFG; writing—review & editing, BZ; funding acquisition, BZ; resources, BZ; supervision, BZ.

Declarations

Conflict of interest The authors declare that they have no conflict of interest.

Ethical approval The collection of patient tissues and data for the generation of organoids and tumors was approved and supervised by the Ethics Committee of the First Affiliated Hospital of Nanchang University (Approval No. CDYFYYLK-04-003; 2023). All procedures followed were in accordance with the ethical standards of the responsible committee on human experimentation and with the Helsinki Declaration of 1975, as revised in 2008(5). Inclusion criteria were a cancer diagnosis, an age of ⩾18 years, and the availability of fresh tissue through biopsy or surgical resection of primary or metastatic lesions. Before surgery, patients were assessed for eligibility and informed consent for participation was obtained.

Data availability The datasets used and/or analyzed during the current study are available from the corresponding author upon request.

References

1. Rossi G, Manfrin A, Lutolf MP (2018) Progress and potential in organoid research. Nat Rev Genet 19(11):671–687. https://doi.org/10.1038/s41576-018-0051-9
2. Dart A (2019) Organoid 2.0. Nat Rev Cancer 19(3):126–127. https://doi.org/10.1038/s41568-019-0108-x
3. Tuveson D, Clevers H (2019) Cancer modeling meets human organoid technology. Science 364(6444):952–955. https://doi.org/10.1126/science.aaw6985
4. Tenreiro MF, Branco MA, Cotovio JP et al (2023) Advancing organoid design through co-emergence, assembly, and bioengineering. Trends Biotechnol 41(7):923–938. https://doi.org/10.1016/j.tibtech.2022.12.021
5. Beydag-Tasöz BS, Yennek S, Grapin-Botton A (2023) Towards a better understanding of diabetes mellitus using organoid models. Nat Rev Endocrinol 19(4):232–248. https://doi.org/10.1038/s41574-022-00797-x
6. Fang Z, Li PJ, Du FY et al (2023) The role of organoids in cancer research. Exp Hematol Oncol 12(1):69. https://doi.org/10.1186/s40164-023-00433-y
7. Piantino M, Figarol A, Matsusaki M (2021) Three-dimensional in vitro models of healthy and tumor brain microvasculature for drug and toxicity screening. Front Toxicol 3:656254. https://doi.org/10.3389/ftox.2021.656254
8. Heinrich MA, Liu W, Jimenez A et al (2019) 3D bioprinting: from benches to translational applications. Small 15(23):e1805510. https://doi.org/10.1002/smll.201805510

9. Park SE, Georgescu A, Huh D (2019) Organoids-on-a-chip. Science 364(6444):960–965. https://doi.org/10.1126/science.aaw7894
10. Du ZC, Mi SL, Yi XM et al (2018) Microfluidic system for modelling 3D tumour invasion into surrounding stroma and drug screening. Biofabrication 10(3):034102. https://doi.org/10.1088/1758-5090/aac70c
11. Wang ZH, Zhang YQ, Li Z et al (2023) Microfluidic brain-on-a-chip: from key technology to system integration and application. Small 19(52):e2304427. https://doi.org/10.1002/smll.202304427
12. Mark D, Haeberle S, Roth G et al (2010) Microfluidic lab-on-a-chip platforms: requirements, characteristics and applications. Chem Soc Rev 39(3):1153–1182. https://doi.org/10.1039/b820557b
13. Huang YS, Huang ZJ, Tang ZM et al (2021) Research progress, challenges, and breakthroughs of organoids as disease models. Front Cell Dev Biol 9:740574. https://doi.org/10.3389/fcell.2021.740574
14. Sobrino A, Phan DTT, Datta R et al (2016) 3D microtumors in vitro supported by perfused vascular networks. Sci Rep 6: 31589. https://doi.org/10.1038/srep31589
15. Grebenyuk S, Abdel Fattah AR, Kumar M et al (2023) Large-scale perfused tissues via synthetic 3D soft microfluidics. Nat Commun 14(1):193. https://doi.org/10.1038/s41467-022-35619-1
16. Voges HK, Foster SR, Reynolds L et al (2023) Vascular cells improve functionality of human cardiac organoids. Cell Rep 42(5):112322. https://doi.org/10.1016/j.celrep.2023.112322
17. Zhang YS, Arneri A, Bersini S et al (2016) Bioprinting 3D microfibrous scaffolds for engineering endothelialized myocardium and heart-on-a-chip. Biomaterials 110:45–59. https://doi.org/10.1016/j.biomaterials.2016.09.003
18. Barlesi F, Gervais R, Lena H et al (2011) Pemetrexed and cisplatin as first-line chemotherapy for advanced non-small-cell lung cancer (NSCLC) with asymptomatic inoperable brain metastases: a multicenter phase II trial (GFPC 07-01). Ann Oncol 22(11): 2466–2470. https://doi.org/10.1093/annonc/mdr003
19. Hong H, Hu ML, Dai LS (2020) Dynamic mechanical behavior of hierarchical resin honeycomb by 3D printing. Polymers 13(1):19. https://doi.org/10.3390/polym13010019
20. Bennett MR, Pang WL, Ostroff NA et al (2008) Metabolic gene regulation in a dynamically changing environment. Nature 454(7208): 1119–1122. https://doi.org/10.1038/nature07211
21. Novo P, Volpetti F, Chu V et al (2013) Control of sequential fluid delivery in a fully autonomous capillary microfluidic device. Lab Chip 13(4):641–645. https://doi.org/10.1039/c2lc41083d
22. Schaefer CF, Anthony K, Krupa S et al (2009) PID: the pathway interaction database. Nucleic Acids Res 37(suppl_1):D674–D679. https://doi.org/10.1093/nar/gkn653
23. Subramanian A, Tamayo P, Mootha VK et al (2005) Gene set enrichment analysis: a knowledge-based approach for interpreting genome-wide expression profiles. Proc Natl Acad Sci USA 102(43):15545–15550. https://doi.org/10.1073/pnas.0506580102
24. Wei JS, Ran G, Wang X et al (2019) Gene manipulation in liver ductal organoids by optimized recombinant adeno-associated virus vectors. J Biol Chem 294(38):14096–14104. https://doi.org/10.1074/jbc.RA119.008616
25. Liu TT, Wang H, Chen YY et al (2023) SENP5 promotes homologous recombination-mediated DNA damage repair in colorectal cancer cells through H2AZ deSUMOylation. J Exp Clin Cancer Res 42(1):234. https://doi.org/10.1186/s13046-023-02789-9
26. Sugihara K, Yamaguchi Y, Usui S et al (2020) A new perfusion culture method with a self-organized capillary network. PLoS ONE 15(10):e0240552. https://doi.org/10.1371/journal.pone.0240552
27. Cucullo L, Hossain M, Tierney W et al (2013) A new dynamic in vitro modular capillaries-venules modular system: cerebrovascular physiology in a box. BMC Neurosci 14:18. https://doi.org/10.1186/1471-2202-14-18
28. Pirker R, Krajnik G, Zöchbauer S et al (1995) Paclitaxel/cisplatin in advanced non-small-cell lung cancer (NSCLC). Ann Oncol 6(8): 833–835. https://doi.org/10.1093/oxfordjournals.annonc.a059324
29. Marx U, Akabane T, Andersson TB et al (2020) Biology-inspired microphysiological systems to advance patient benefit and animal welfare in drug development. ALTEX 37(3):365–394. https://doi.org/10.14573/altex.2001241
30. Murphy AR, Campo H, Kim JJ (2022) Strategies for modelling endometrial diseases. Nat Rev Endocrinol 18(12):727–743. https://doi.org/10.1038/s41574-022-00725-z
31. Shinha K, Nihei W, Nakamura H et al (2021) A kinetic pump integrated microfluidic plate (KIM-plate) with high usability for cell culture-based multiorgan microphysiological systems. Micromachines 12(9):1007. https://doi.org/10.3390/mi12091007
32. Pabla N, Dong Z (2008) Cisplatin nephrotoxicity: mechanisms and renoprotective strategies. Kidney Int 73(9):994–1007. https://doi.org/10.1038/sj.ki.5002786